Open Access

Catalysis Research

LIDSEN Publishing Inc.

Original Research

Fischer-Tropsch Synthesis on Co/SBA-15 Catalyst: Characterization and Oligomerization Modeling

Virginia M. R. Menezes [1, †], Gustavo M. Paula [2, †], Liliane A. Lima [2, †], Meiry G. F. Rodrigues [2, †], Fabiano A. N. Fernandes [1, *]

1. Universidade Federal do Ceará, Departamento de Engenharia Química, Campus do Pici, Bloco 709, 60455-760 Fortaleza – CE, Brazil; E-Mails: virginia.any@gmail.com; fabiano@ufc.br
2. Universidade Federal de Campina Grande, Departamento de Engenharia Química, 58109-970 Campina Grande - PB, Brazil; E-Mails: gustafpaula@hotmail.com; liliandradelima@yahoo.com.br; meiry@deq.ufcg.edu.br

† These authors contributed equally to this work.

* **Correspondence:** Fabiano A. N. Fernandes; E-Mail: fabiano@ufc.br

Academic Editor: Shouquan Huo

Special Issue: Recent Progress and Development in Iron and/or Cobalt Catalysis

Catalysis Research
2022, volume 2, issue 3
doi:10.21926/cr.2203023

Received: May 05, 2022
Accepted: August 07, 2022
Published: August 16, 2022

Abstract

In this study, we investigated the oligomerization mechanism of the Fischer-Tropsch synthesis catalyzed by a cobalt-based catalyst supported by SBA-15. The Co/SBA-15 catalyst contained 20% w/w of cobalt. It was prepared by the wet impregnation method and characterized by X-ray diffraction (XRD), N_2 adsorption-desorption, temperature-programmed reduction (TPR), and scanning electron microscopy coupled to X-ray energy dispersion spectroscopy (SEM-EDS). The FT synthesis was conducted in a slurry bed reactor operating at 240–270°C, 2.0–3.0 MPa, and 1:1–2:1 H_2:CO ratio (mol:mol). An oligomerization model, based on alkyl and alkenyl mechanisms for hydrocarbon chain propagation, was used for product distribution. Impregnation with cobalt and calcination did not alter the structure of SBA-15. Cobalt oxides, including Co_2O_3 and Co_3O_4, were the active phases of the reaction. Adding cobalt to the

support lowered the specific surface area and the pore volume of the support but did not change the structure of SBA-15. Fischer-Tropsch synthesis and C^{5+} hydrocarbon selectivity increased at a low H_2:CO ratio (1.0) and low temperatures (240–255°C). The content of branched-chain paraffin and olefins increased with a decrease in the H_2:CO ratio and temperature. The parameters of the model were estimated, and the assumption of a dual mechanism was satisfied.

Keywords
Fischer-Tropsch synthesis; SBA; cobalt-based catalyst; liquid fuels; reaction mechanism

1. Introduction

Natural gas can be converted to synthesis gas (a mixture of CO and H_2) and then to liquid fuels, including hydrocarbons (paraffin and olefins), and energy by the Fischer-Tropsch Synthesis (FTS). Several plants apply FTS to produce liquid fuels with low sulfur, aromatic, and oxygenated content [1].

The type of catalyst strongly influences the specific hydrocarbon distribution and the productivity of synthesis. Many studies have discussed the advantages and disadvantages of using cobalt or iron-based catalysts for producing paraffin and olefins [1-4]. The carbon number distribution obtained using Co-based catalysts is affected by the reducibility of the cobalt oxides, the type of support, and the average pore size [1-4]. Different cobalt-based catalysts have different reaction rates and yields and catalyze the formation of different products (hydrocarbon distribution).

Many supports have been developed for cobalt catalysts used in FTS. Silica, alumina, molecular sieves, and zeolites are the most studied supports for Co-based FTS catalysts. Porous supports guarantee a uniform dispersion of active metal particles in the catalyst and protect it from agglomeration. Porous SBA materials are suitable for supporting FTS because of their satisfactory chemical stability and thermal conductivity [5-8].

The mesoporous silica-based material SBA-15 has uniform hexagonal channels with narrow and uniform pores. It also facilitates higher active metal dispersion inside the support. It has high stability and a large surface area (500–1,000 m^2/g) [7, 9-12]. The textural and morphological characteristics of SBA-15 allow it to support FTS catalysts.

The activity of FTS catalysts depends on the concentration of the surface metal, its dispersion on the support, and the degree of reduction of metal oxides. A limitation of silica-based supports for cobalt catalysts is that the interaction between Co and SiO_2 is weak (e.g., for Co and TiO_2). It tends to form metal agglomerates, resulting in a low metal dispersion on the support [13, 14]. SBA-15 promotes the functional interaction between cobalt and SiO_2 owing to its highly ordered pore texture. The structure limits the formation of cobalt aggregates and improves their dispersion on the support. Cobalt oxide particles are highly reducible when supported by silica-based materials and show a large number of active sites [13].

The product distribution generated by Co-based catalysts depends mainly on the reaction conditions and the applied reaction technique. The FT reaction is usually conducted in a slurry or tubular reactor, which operates at temperatures and pressures ranging from 240 to 270°C and 1 to

4 MPa, respectively [15]. The choice of the reactor technology affects product distribution because it determines the concentration gradient of H_2 and CO in the reactor, the reaction phase, and the active site [16-19].

In this study, we investigated the oligomerization mechanism of the Fischer-Tropsch synthesis catalyzed by 20% (w/w) cobalt supported on SBA-15. We also characterized the Co-based catalyst supported on SBA-15 and evaluated the selectivity of the FTS products synthesized under different operating conditions in a slurry reactor. In this study, a phenomenological mathematical model was used for the first time to determine the reaction steps most affected by changes in the operating conditions. To evaluate the effects of the operating conditions at each reaction step, a mathematical model was used, assuming the co-occurrence of alkyl and alkenyl mechanisms during FTS. The kinetic parameters of the reaction were determined to identify the reaction steps that were more susceptible to variations in this cobalt-based catalyst.

2. Materials and Methods

2.1 Synthesis of SBA-15

The SBA-15 material was synthesized following the procedure reported by Zhao [10], using a reaction mixture with a molar composition of 1.0 SiO_2/0.017 P123/5.7 HCl/193 H_2O. Pluronic P123 (P123, $EO_{20}PO_{70}EO_{20}$) was dissolved in a solution of HCl (2 mol/L) and stirred for 4 h at 35°C. Tetraethyl orthosilicate (TEOS, 98%) was added to the mixture and stirred for 24 h at 35°C. The obtained mixture was treated by the conventional hydrothermal method for 48 h at 100°C. The product was centrifuged at 1,100 rpm, washed with deionized water, and dried at 60°C for 24 h. The material was calcined in static air at 550°C for 7 h to remove the polymer matrix (P123).

2.2 Synthesis of the Co/SBA-15 Catalyst

Cobalt was deposited on the SBA-15 support by applying the wet impregnation method. The catalyst produced had 20% cobalt (w/w) on SBA-15. A cobalt nitrate solution [$Co(NO_3)_2{\cdot}6H_2O$] (0.1 mol/L) was added gradually to the SBA-15 support. The suspension was stirred at room temperature for 30 min.

The mixture was dried at 100°C for 24 h. The solid material was calcined from room temperature to 200°C under a stream of nitrogen (flow rate: 100 mL/min). The temperature was increased by 10°C/min. The final temperature was maintained for 1 h. Then, nitrogen was replaced by synthetic air and heated at 2°C/min from 200 to 450°C; the treatment continued at this temperature for 2 h.

2.3 Characterization of the Catalyst

Powder diffraction patterns were measured through X-ray diffraction (XRD) using a Shimadzu XRD 6000 instrument, where Cu-Kα irradiation was applied at 40 kV/30 mA, and a goniometer velocity of 2°/min was maintained with a step size of 0.02° over the 2θ range from 0.5° to 10° and 20° to 80°. The phases were identified by the Rietveld refinement method and compared to the data from the Joint Committee on Powder Diffraction Standards (JCPDS) database. The average diameter of the sample crystallites was determined using the Scherrer equation.

Elemental analysis was conducted by performing energy-dispersive X-ray spectrophotometry in a Shimadzu EDX-700 instrument.

The textural characteristics of the samples were investigated by isothermal gas adsorption/desorption of N_2 at –196°C using a Micromeritics ASAP 2020 adsorption analyzer. The adsorption and desorption N_2 isotherms were obtained at relative pressures (P/P_0) between 0.06 and 0.98. The BET method was used to determine the average pore diameter and surface area (SBET). The external surface area (SE), micropore area (SM), and the average volume of the micropores (VM) were determined by the t-plot method. The BJH method was used to calculate the average pore volume (VP) and the average pore diameter (DP).

The calcined catalyst was characterized by TPR using a Micromeritics ChemiSorb 2720 instrument under a mixed flow of H_2-N_2 (5% H_2 at 30 mL/min). Approximately 20 mg of the catalyst was pre-treated and heated from room temperature to 200°C (at 10°C/min). It was maintained at this temperature for 1 h under a stream of nitrogen (flow rate: 30 mL/min). The sample was cooled, and the data were collected. The catalyst was heated from 20°C to 1,000°C at 10°C/min.

The SEM images were recorded using a Shimadzu (model SSx 550) scanning electron microscope at an acceleration voltage of 20 kV. Elemental analysis was conducted by energy dispersive X-ray spectrophotometry (EDX) using a Shimadzu EDX-700 instrument. The solids were prepared by sputtering Au on their surfaces.

The TEM images were taken using a JEOL JEM-1200 EX electron microscope. The samples were prepared by dispersing the solids in alcoholic solutions and dropping them on a carbon-coated copper grid. Finally, the samples were air-dried and characterized.

2.4 Fischer-Tropsch Synthesis

The Fischer-Tropsch synthesis was conducted in a high-pressure autoclave reactor (Parr model 4571; 400 mL) using 2.0 g of the catalyst. The synthesis gas was prepared by mixing H_2 and CO using two mass flow controllers (Alborg GFC-17). The synthesis gas was fed into the reactor below the agitator. The reaction was conducted under constant mechanical agitation (800 rpm). The reactions were performed with 2.0 g of Co/SBA-15 catalyst suspended in 200 mL of hexadecane (slurry phase). A gas entrainment impeller was used to constantly recirculate the syngas from the headspace into the slurry phase. The catalyst was activated in situ at 240°C and 2.0 MPa for 6 h under an atmosphere of CO and H_2 (H_2:CO ratio = 1.0). The operating conditions of the catalytic tests included a total pressure of 2–3 MPa, a temperature of 240–270°C, and an H_2:CO feed ratio of 1.0 and 2.0 [20, 21].

The effluent gas from the reactor was analyzed using a gas chromatograph (Thermos model Ultra) equipped with an ionic barrier detector (BID) and a flame-ionization detector (FID). A Carboxen 1006 Plot capillary column (30 m × 0.25 mm i.d. × 0.25 µm film) followed by an RTX-1 capillary column (30 m × 0.25 mm i.d. × 0.25 µm film) were used to separate the hydrocarbon products. A specific temperature program (30 to 60°C) was used during separation to identify the gaseous Fischer-Tropsch products (C_1 to C_8), hydrogen, carbon monoxide, and carbon dioxide.

The liquid product was analyzed online by a gas chromatograph (Thermos model Ultra) equipped with a flame-ionization detector (FID). A specific temperature program (30 to 280°C) was used with an OV-5 capillary column (30 m × 0.25 mm i.d. × 0.25 µm film) to identify the liquid Fischer-Tropsch products (C_4 to C_{14}). The conversions were obtained based on the syngas mass balance of CO.

2.5 Uncertainty Analysis

The data were presented as the mean ±standard deviation. The measurement uncertainty replaced the standard deviation whenever the measurement or process uncertainty was higher than the standard deviation of the triplicate.

2.6 FTS Oligomerization Modeling

The model used in this study was based on the oligomerization model presented in Fontenelle & Fernandes [22]. The overall reaction rate assumed that both reactants were adsorbed on the catalyst before they reacted to form the *in situ* monomer CH_2 (Equation 1). The formation of the monomer was independent of the hydrocarbon chain length, given its formation in a free active site.

$$R_{FTS} = \frac{k_{FTS1} \cdot P_{CO} \cdot (P_{H2})^{k_{FTS2}}}{(1 + k_{FTS3} \cdot P_{CO} + k_{FTS4} \cdot P_{H2})^2} \quad (1)$$

The model assumed that the oligomerization of CH_2 occurs through a dual mechanism (alkyl and alkenyl) and has three steps, including initiation, propagation, and termination. The mass balances for the Fischer-Tropsch oligomerization reaction are shown in Equations 2 to 12. A full description of the development of the model is provided in Fontenelle & Fernandes [22].

$$R(1) = \frac{k_i \cdot R_{FTS} \cdot P_{H2}^{0.5}}{k_{p1} \cdot R_{FTS} + k_{met} \cdot P_{H2}^{0.5}} \quad (2)$$

$$R(2) = \frac{k_{p1} \cdot R_{FTS} \cdot R(1) + k_{ads} \cdot P_{H2}^{0.5} \cdot P^{=}(2)}{k_p \cdot R_{FTS} + k_{par} \cdot P_{H2}^{0.5}} \quad (3)$$

$$R''(2) = \frac{k_{i2} \cdot R_{FTS}}{k_{p2}} \quad (4)$$

$$R''(3) = \frac{k_{p2} \cdot R_{FTS} \cdot R''(2)}{k_{p2} \cdot R_{FTS} + k_{olef2} \cdot P_{H2}^{0.5}} \quad (5)$$

$$R(n) = \frac{k_p \cdot R_{FTS} \cdot R(n-1) + k_{ads} \cdot P_{H2}^{0.5} \cdot P^{=}(n)}{k_p \cdot R_{FTS} + k_{par} \cdot P_{H2}^{0.5} + k_{olef}} \quad (6)$$

$$R''(n) = \frac{k_{p2} \cdot R_{FTS} \cdot R''(n-1)}{k_{p2} \cdot R_{FTS} + k_{olef2} \cdot P_{H2}^{0.5}} \quad (7)$$

$$\frac{dP(1)}{dt} = k_{met} \cdot P_{H2}^{0.5} \cdot R(1) \quad (8)$$

$$\frac{dP(2)}{dt} = k_{et} \cdot P_{H2}^{0.5} \cdot R(2) \quad (9)$$

$$\frac{dP^{=}(2)}{dt} = k_{O2} \cdot {R_{FTS}}^2 \quad (10)$$

$$\frac{dP(n)}{dt} = k_{par} \cdot P_{H2}^{0.5} \cdot R(n) \quad (11)$$

$$\frac{dP^{=}(n)}{dt} = k_{olef} \cdot R(n) + k_{olef2} \cdot P_{H2}^{0.5} \cdot R''(n) - k_{ads} \cdot P_{H2}^{0.5} \cdot P^{=}(n) \quad (12)$$

The Arrhenius equation was applied to account for the kinetic parameters of the model (Equation 13).

$$k_i = A\ exp\left(\frac{-E_{ai}}{RT}\right) \quad (13)$$

Seven sets of experimental data were used to fit the parameters of the model, and three sets of experimental data were used for model validation. The kinetic parameters were estimated using an algorithm developed in Python based on the Trust Region Reflective method to minimize the sum of squared errors. Several sets of initial parameters were tested to determine if the kinetic parameters referred to a global optimum.

3. Results and Discussion

3.1 Chemical Composition and Textural Properties of the Support and the Catalyst

The diffractograms of the SBA-15 presented three peaks, which were located at 2θ = 0.9°, 1.5°, and 1.7° (Figure 1a). These peaks corresponded to the crystalline planes with the Miller index (1 0 0), (1 1 0), and (2 0 0), respectively. The reflections conformed to the p6 mm hexagonal symmetry. This characteristic of SBA-15 matched the characteristics reported by several authors for mesoporous SBA-15 [10, 23, 24].

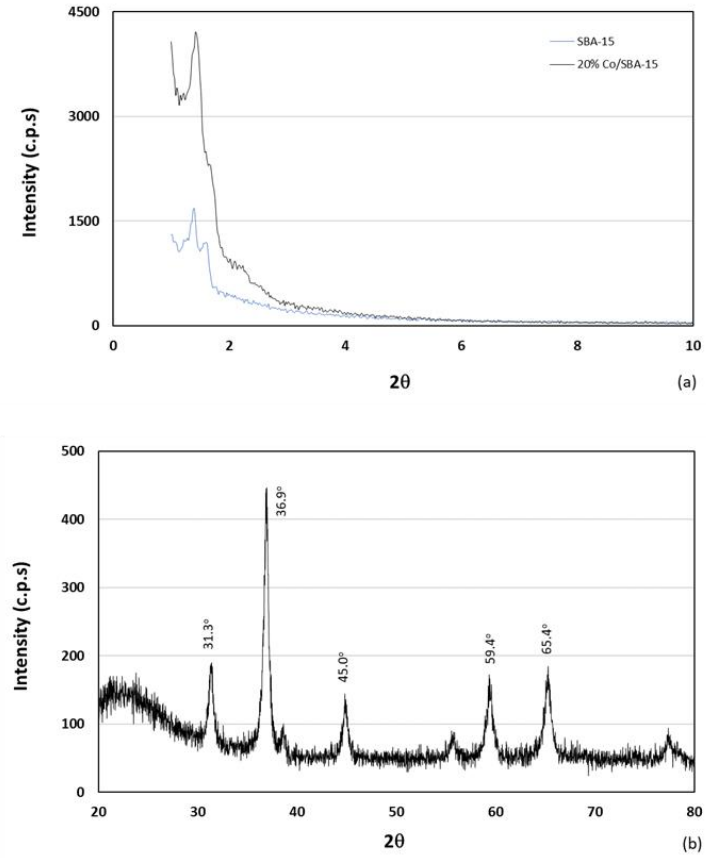

Figure 1 The diffractogram of (a) the SBA-15 molecular sieve and the 20% Co/SBA-15 catalyst at 2θ = 0.5° to 10° (b) and 2θ = 25° to 80°.

The calcined Co/SBA-15 catalyst diffractogram showed peaks at 2θ = 0.9° and 1.5° (Figure 1a). The diffractogram showed that the impregnation of the support with cobalt nitrate and its transformation into cobalt oxides slightly changed the support structure. This result agreed with the characteristics reported by several authors for other oxides supported by SBA-15 [25-27].

The crystalline cobalt oxide phases (Figure 1) were identified using the crystallographic charts for these oxides (available in the JCPDS-ICDD library). The decomposition of cobalt nitrate [$Co(NO_3)_2 \cdot 6H_2O$] produced a mixture of Co_2O_3 and Co_3O_4, identified by the peaks at 2θ = 31.3, 36.9, 45.1, 59.4, and 65.4 on the calcined catalyst.

The d_{100} interplanar spaces and the a_0 unit cell parameters for the support and catalyst are shown in Table 1. The support analysis showed values that were similar to those reported in other studies on SBA-15 [25-27]. The unit cell parameter of the catalyst decreased slightly, denoting that the mesoporous structure of the support remained unaltered after impregnation and calcination.

Table 1 The interplanar spaces and unit cell parameters for the support and the catalyst.

Sample	2θ	$d_{(100)}$ (nm)	a_0 (nm)
SBA-15	0.95 ±0.01	9.3 ±0.1	10.74 ±0.11
20% Co/SBA-15	0.97 ±0.01	9.1 ±0.1	10.50 ±0.11

The results of the chemical analysis of the catalyst (Table 2) showed that the impregnation of the support was successful, and the catalyst had the designed mass fraction of cobalt. The SBA-15

support consisted primarily of silica, as expected for this kind of support [27, 28], and after impregnation, the catalyst consisted of silica and cobalt oxide.

Table 2 The chemical composition of the SBA-15 support and the Co/SBA-15 catalyst.

Sample	SiO_2 (%)	Co_2O_3 (%)	Other (%)
SBA-15	99.3 ±0.3	-	0.7 ±0.1
20% Co/SBA-15	72.8 ±0.3	27.1 ±0.1	0.1 ±0.1

The N_2 adsorption-desorption isotherms of the support and the catalyst exhibited a typical type IV isotherm with H1-type hysteresis loops (Figure 2), which is characteristic of several ordered mesoporous materials. Adsorption to the support occurred in a monolayer at low pressure ($P/P_0 < 0.6$), as capillary condensation at P/P_0 values between 0.6 and 0.9, and in multiple layers at $P/P_0 > 0.9$. The sharp inflection at a relative pressure of 0.7 to 0.8 indicated that the SBA-15 support had uniform mesopores [29, 30].

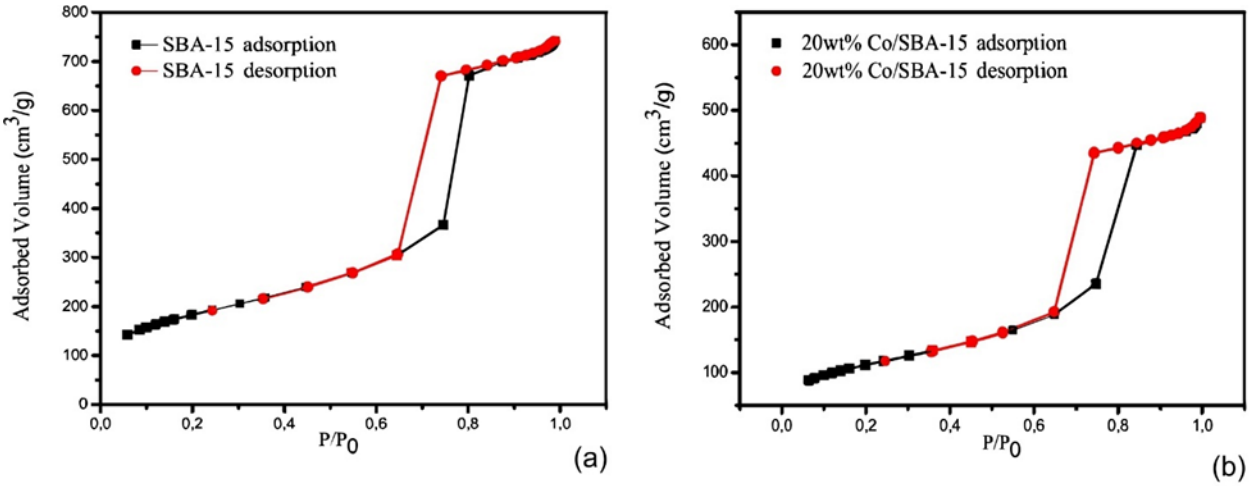

Figure 2 The N_2 adsorption and desorption isotherms (at –196°C) of SBA-15 (a) and the 20% Co/SBA-15 catalyst (b).

Adsorption onto the surface of the catalyst occurred in a monolayer at low pressure ($P/P_0 < 0.6$), as capillary condensation at P/P_0 values between 0.6 and 0.85, and in multiple layers at $P/P_0 > 0.85$ [31-33]. The similarity of the isotherms indicated that the pore structure of the support was preserved after cobalt deposition. The height of the hysteresis loop decreased slightly after impregnation, suggesting that the mesopores were partly blocked due to cobalt deposition.

3.2 Surface and Morphological Analyses

The support structure had silica fibers with micrometric dimensions formed through the linear adhesion of sub-micrometric particles (Figure 3). The textural properties of the support are shown in Table 3. The catalyst had an average pore volume (VP) and superficial area lower than those of the support due to the partial loading of the pores with cobalt oxides. The pore volume decreased by 33%, and the surface area decreased by 39%.

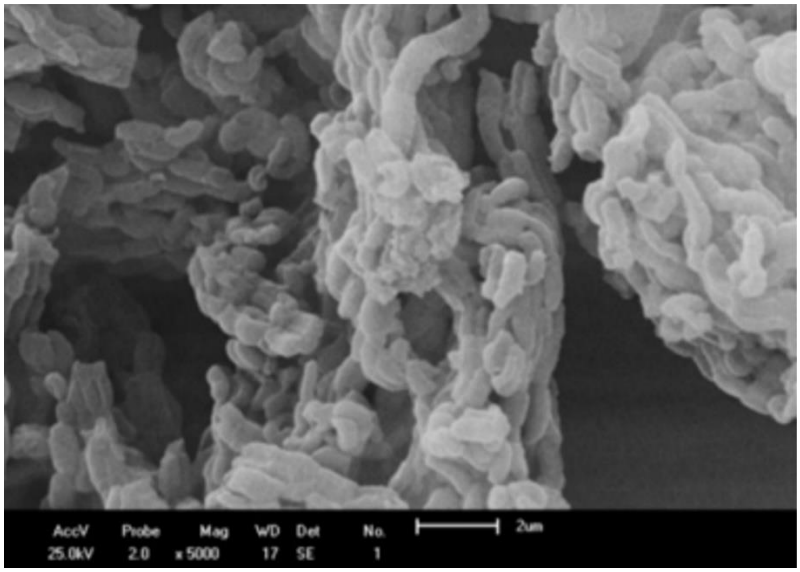

Figure 3 The MEV micrographs of the SBA-15 support (magnification: 5,000×).

Table 3 The textural analysis of SBA-15 and the Co/SBA-15 catalyst.

Samples	S_{BET} (m^2/g)	S_{ext} (m^2/g)	S_{micro} (m^2/g)	V_p (cm^3/g)	V_{micro} (cm^3/g)	D_P (nm)
SBA-15	660 ±7	589 ±6	71 ±1	1.16 ±0.01	0.03 ±0.00	7.2 ±0.1
20% Co/SBA-15	402 ±5	400 ±5	46 ±1	0.77 ±0.01	0.02 ±0.00	7.8 ±0.1

S_{BET}: superficial area calculated by the BET method; S_{ext}: external surface area calculated by the t-Plot method; S_{micro}: micropore area calculated by the t-Plot method; V_P: average pore volume calculated by the BJH method; V_{micro}: average micropores volume calculated by the t-Plot method; D_P: average pore diameter calculated by the BJH method.

The transmission electron micrographs of the catalyst are shown in Figure 4. The micrographs showed small dark regions dispersed in a hexagonal channel structure (indicated by the arrows). The dark areas were formed by reduced cobalt particles, which agglomerated in an isle-like shape in the support. The micrographs suggested that impregnation with cobalt nitrate or calcination did not damage the SBA-15 support. The micrographs also indicated that the cobalt particles were evenly distributed on the support, but only some channels were filled with the cobalt particles [7, 12, 34].

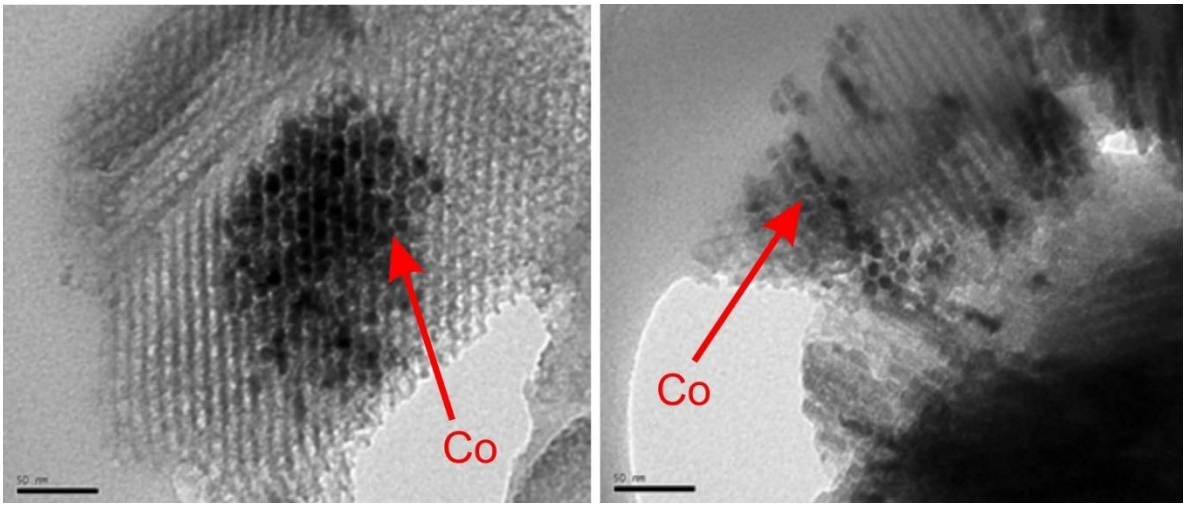

Figure 4 Transmission electron micrographs of the 20% Co/SBA-15 catalyst.

3.3 Temperature-programmed reduction (TPR) pattern

The reduction pattern of the Co/SBA-15 catalyst is shown in Figure 5. The TPR pattern showed three reduction peaks at 150, 280, and 316°C. The first reduction peak corresponded to the decomposition of cobalt nitrate, which remained in the catalyst after calcination. The second reduction peak corresponded to the reduction of Co_3O_4 and Co_2O_3 to CoO and Co^0. The third reduction peak corresponded to inactive cobalt silicates (Co_2SiO_4) produced due to a strong interaction between cobalt and the silica of the SBA-15 support [12, 34].

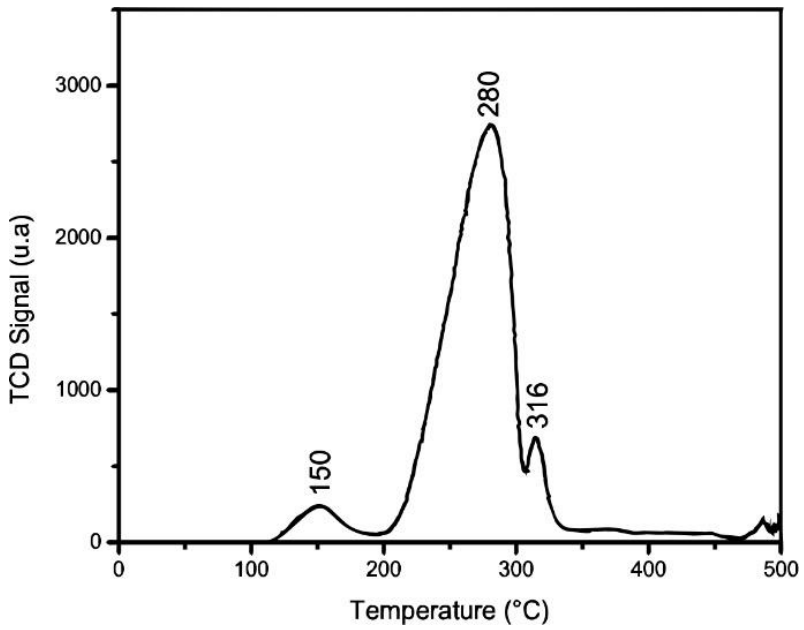

Figure 5 The TPR profile of the 20% Co/SBA-15 catalyst.

3.4 Catalytic Evaluation in FTS

The catalytic data for the FTS catalyst developed in this study is shown in Table 4. The entire quantity of CO was converted into hydrocarbons because of the low flow rate applied, which aimed

at high CO conversion and high catalyst activity. The activity of the 20% Co/SBA-15 catalyst was higher than that of other catalysts tested previously by our group. Those catalysts usually had a conversion rate of 30% to 60% under the same reaction conditions [7, 12, 26, 35, 36]. The conversion observed here was higher than that obtained when small differential tubular reactors were used because the catalyst used had a higher mass. The reactor configuration allowed gas recirculation through the slurry containing the catalyst.

Table 4 The catalytic test of the 20% Co/SBA-15 catalyst.

Temperature (°C)	Pressure (MPa)	H_2:CO (mol/mol)	C_1 (% wt)	C_2-C_4 (% wt)	C_5-C_9 (% wt)	C_{10+} (% wt)
240	2.0	1.0	6.4 ±0.3	32.7 ±3.3	46.6 ±9.3	14.3 ±2.9
240	3.0	1.0	6.9 ±0.3	35.2 ±3.5	43.0 ±8.6	15.0 ±3.0
255	2.5	1.0	8.1 ±0.4	37.3 ±3.7	44.5 ±8.9	10.1 ±2.0
270	2.0	1.0	23.1 ±1.1	38.7 ±4.0	32.8 ±6.6	5.4 ±1.1
270	3.0	1.0	20.0 ±1.0	42.0 ±4.1	34.1 ±6.8	3.9 ±0.8
240	2.0	2.0	27.4 ±1.4	37.3 ±3.7	25.5 ±5.1	9.7 ±2.0
240	3.0	2.0	64.0 ±3.2	29.9 ±3.0	4.8 ±1.0	1.4 ±0.3
255	2.5	2.0	60.7 ±3.0	27.5 ±2.7	8.6 ±1.7	3.1 ±0.6
270	2.0	2.0	65.0 ±3.2	29.3 ±2.9	3.9 ±0.8	1.8 ±0.4
270	3.0	2.0	62.4 ±3.1	29.8 ±3.0	4.6 ±1.0	3.1 ±0.6

The distribution of the product depended on the reaction conditions, especially the ratio of hydrogen to carbon monoxide. The C_5–C_9 hydrocarbons were the main products of FTS on the 20% Co/SBA-15 catalyst when the reaction was conducted at a low H_2:CO molar ratio (1.0) and low temperature (≤255°C). When the molar ratio increased to 2.0, the main product formed was methane, except for when the reaction was conducted at 240°C and 2.0 MPa, in which case the main product was the C_2-C_4 fraction.

The catalyst produced more C^{5+} hydrocarbons at low temperatures (240°C) and low pressures (2.0 MPa). The amount of C^{10+} hydrocarbons was higher at a low H_2:CO ratio because lower hydrogen concentration was present in the reaction media, which corroborated with the role of hydrogen as a reactant and a chain transfer agent.

A reduction in the C^{5+} content and a significant increase in methane were observed when the H_2:CO ratio, temperature, and pressure increased. In such cases, the reduction of the hydrocarbon chain length was associated with an increase in hydrogen concentration and reaction temperature. Under such conditions, the chain transfer reaction, which halts the propagation of CH_2 units, increased, resulting in the formation of hydrocarbons with low molecular weight.

A significant reduction in methane and selectivity toward C^{5+} products displayed by the catalyst confirmed the role of SBA as support for providing suitable catalytic activity and high selectivity to the Co-based catalyst. The performance of the catalyst in producing heavy hydrocarbons (C^{10+}) might be related to the higher surface area and mean pore diameter of the catalyst, which can further enhance the growth of the hydrocarbon chain.

A decrease in the ratio of H_2:CO increased the fraction of olefins and branched-chain paraffin (Table 5). The termination of hydrocarbon chains to olefins was independent of the concentration

of hydrogen. In contrast, the termination of hydrocarbon chains to paraffin was directly related to the hydrogen concentration in the active site of the catalyst [22]. As the concentration of hydrogen decreased, the termination to olefins increased proportionally, producing more olefins. The readsorption of olefins, followed by termination to paraffin, produced branched-chain paraffin [37]. Since more olefins were generated in hydrogen-poor media, more branched-chain paraffin was produced in our experiment.

Table 5 The characteristics of the liquid product (C_{5+}).

Temperature (°C)	Pressure (MPa)	H_2:CO (mol/mol)	Branched Paraffins (%)	Olefins (%)
240	2.0	1.0	14.4 ±2.9	14.0 ±2.8
240	3.0	1.0	12.6 ±2.5	13.6 ±2.7
255	2.5	1.0	13.0 ±2.6	11.4 ±2.3
270	2.0	1.0	11.1 ±2.2	10.2 ±2.0
270	3.0	1.0	13.0 ±2.6	10.5 ±2.1
240	2.0	2.0	9.2 ±1.8	12.7 ±2.5
240	3.0	2.0	6.0 ±1.2	10.0 ±2.0
255	2.5	2.0	8.6 ±1.7	8.6 ±1.7
270	2.0	2.0	7.7 ±1.5	9.2 ±1.8
270	3.0	2.0	8.4 ±1.7	8.4 ±1.6

The FTS conducted in the slurry reactor showed a good selectivity of C^{5+} hydrocarbons (60.9 ±9.3%), higher olefin production (14.0 ±2.8%), and lower methane formation (6.4 ±0.3%) compared to the FTS conducted in tubular reactors under similar operating conditions and using the same catalyst. The FTS showed 75.9% C^{5+} hydrocarbons in tubular reactors, 0.4% olefin, and 16.9% methane (w/w) [9]. Another study on 20% Co/SBA-15 catalyst [38] in tubular reactors also showed similar C^{5+} selectivity (64.7%) and olefin production (10.5%).

High methane selectivity was reported for low-loaded Co catalysts with high dispersion and low reducibility [39]. Unreduced cobalt oxides catalyze the water-gas-shift (WGS) reaction favoring hydrogenation reactions, which is the primary cause of high methane selectivity. The catalyst studied here was not active for the WGS reaction and showed low selectivity for methane, indicating that it contained low levels of unreduced cobalt oxides.

The comparison of the 20% Co/SBA-15 catalyst with other cobalt catalysts used in other studies showed that the catalyst reported here was productive at low temperatures and a low molar ratio of hydrogen to carbon. The 15% Co/SiO_2 catalyst reported by Shiba et al. [40] showed higher C^{5+} selectivity (75%) but also had higher CH_4 selectivity (18%), indicating a narrower hydrocarbon distribution than the 20% Co/SBA-15 catalyst. The Ru-promoted 15% Co/SiO_2 catalyst, also reported by Shiba et al. [40], performed better and showed higher C^{5+} selectivity (90%) and a broader distribution of hydrocarbons.

The Mo-promoted and Pt-promoted Co/TiO_2 catalyst reported by Gahtori et al. [41] showed similar C^{5+} selectivity (62%) compared to the 20% Co/SBA-15 catalyst only at lower temperatures (<180°C) but at the expense of very low carbon monoxide conversion (20%). The cobalt-based mesoporous catalyst developed by Oliveira et al. [42] showed better C^{5+} selectivity (81%) than the

20% Co/SBA-15 catalyst at similar operating conditions (210°C, 1.0 H_2:CO ratio). Similar to the 20% Co/SBA-15 catalyst, the cobalt-based mesoporous catalyst showed a substantial decrease in performance at high temperatures and a high H_2:CO molar ratio.

3.5 Reaction Mechanism and Modeling

The kinetic parameters estimated for the FTS oligomerization reaction are shown in Table 6. The dual mechanism model was well-fitted to the experimental data, as shown in Figure 6.

Table 6 The kinetic parameters for the FTS oligomerization based on the dual mechanism model

Parameter		Pre-exponential coefficient	Activation Energy (J/mol)
Methylene formation (mol.MPa^{-kFTS2}.h^{-1})	k_{FTS1}	2.32×10^{-2}	1.37
Reaction exponent (adm)	k_{FTS2}	0	--
CO adsorption coefficient (MPa^{-1})	k_{FTS3}	6.43×10^{-1}	2.43
H_2 adsorption coefficient (MPa^{-1})	k_{FTS4}	3.93×10^{-1}	3.31
Alkyl mechanism			
Initiation (h.MPa$^{-0.5}$.mol^{-1})	k_i	2.75×10^{5}	11.10
Propagation (h.mol^{-1})	k_p	1.31×10^{-1}	5.62
Termination to paraffin (mol.MPa$^{-0.5}$.h^{-1})	k_{par}	7.37×10^{-5}	1.58
Termination to olefin (mol.h^{-1})	k_{olef}	1.11×10^{-4}	4.96
Termination to methane (mol.MPa$^{-0.5}$.h^{-1})	k_{met}	3.61×10^{-2}	2.55
Termination to ethane (mol.MPa$^{-0.5}$.h^{-1})	k_{et}	5.62×10^{-6}	2.74
Alkenyl mechanism			
Initiation (h.mol^{-1})	k_{i2}	1.96×10^{2}	4.96
Propagation (h.mol^{-1})	k_{p2}	9.50×10^{2}	2.28
Termination to olefin (mol.MPa$^{-0.5}$.h^{-1})	k_{olef2}	1.11×10^{-4}	20.29
Adsorption of olefin (mol.MPa$^{-0.5}$.h^{-1})	k_{ads}	8.61×10^{-2}	0.70
Termination to ethene (h.mol^{-1})	$k_{et\,=}$	8.45×10^{7}	0.75

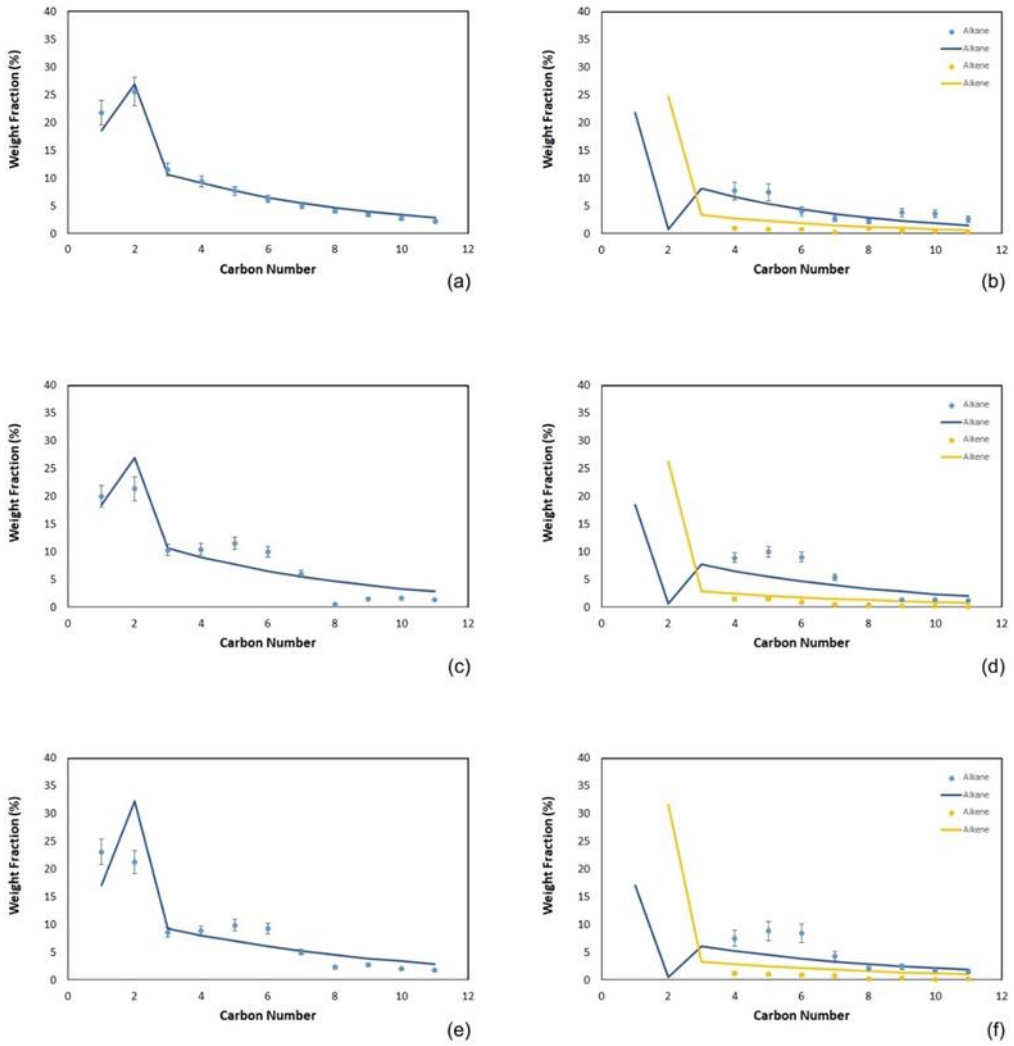

Figure 6 Validation of the mathematical model and comparison between experimental data and model prediction. (a and b) H_2:CO = 2:1, 20 atm, 240°C; (c and d) H_2:CO = 1:1, 30 atm, 270°C; H_2:CO = 1:1, 30 atm, 240°C.

The model was validated against data that were not presented to the model while conducting parameter estimation. The R^2 of the predictions indicated that the model prediction of paraffin and olefin products agreed with the experimental data within the 75% confidence level (Figure 6). The proposed model showed better agreement with the experimental data, especially when the ASF distribution theory failed to predict the distribution. More complex factors, such as the non-uniformity of pore size and diameter that limit mass transfer, might allow the deviation between the predicted model and the experimental data to be incorporated into the model.

The alkane (paraffin) content was significantly higher than the alkene content (olefins) from C_1 to C_{11} except for in C_2. This is because the amount of ethene is usually higher than that of ethane in several Fischer-Tropsch applications. The catalyst predominantly used the alkyl mechanism, indicated by the considerably higher initiation rate for the alkyl mechanism than the alkenyl mechanism.

Among olefins, the ethene content was substantially higher than the content of other alkenes with a higher carbon number, which was also indicated by the higher formation rate of ethene than the termination rate of olefin. The termination rates for olefin in both mechanisms were slightly higher than the termination rate for paraffin, even though the concentration of alkanes was higher than that of alkenes. The results of the analyzed model showed that this catalyst might be re-adsorbing olefins and terminating them as paraffin, following a mechanism already established for the cobalt-based catalyst.

4. Conclusions

The mesoporous SBA-15 support showed well-ordered hexagonal arrays of mesopores with a 2-D hexagonal (P6 mm) mesostructure, which remained unchanged after incorporating the metal. The 20% Co/SBA-15 catalyst produced sufficient levels of C^{5+} hydrocarbons at low temperatures (<255°C) and a low H_2:CO molar ratio (1.0).

The operating conditions strongly influenced the performance of the catalyst, particularly product distribution. The C^{5+} content ranged from 6.2% to 60.9%, which was unfavorable since a more stable performance was desired. The production of branched hydrocarbons and olefins was slightly higher when the H_2:CO ratio was 1.0.

The oligomerization model provided satisfactory predictions, although intraparticle mass transfer limited the ability to make better predictions. However, evaluating the oligomerization model parameters provided a better understanding of the reaction steps regarding where improvements in the catalyst are required. The 20% Co/SBA-15 catalyst showed a high rate constant for termination to methane and low activation energy for this reaction step, compared to the rate constant and activation energy of the propagation step; this was the main problem with the catalyst. Incorporating other metals that can diminish the rate constant for termination to methane might enhance the effectiveness of the catalyst.

Acknowledgments

The authors thank the financial support of the Brazilian funding agencies CNPq and CAPES, Petrobras, and ANP/PRH-25.

Author Contributions

Virginia M. R. Menezes: Investigation, Gustavo M. Paula: Investigation, Formal analysis, Writing – Original Draft; Liliane A. Lima: Investigation, Formal analysis; Meiry G. F. Rodrigues: Conceptualization, Formal analysis, Methodology; Fabiano A. N. Fernandes: Conceptualization, Formal analysis, Funding acquisition, Writing – Review & Editing.

Funding

Conselho Nacional de Desenvolvimento Cientifico e Tecnológico (CNPq); Coordenação de Aperfeiçoamento de Pessoal de Nível Superior (CAPES); Agencia Nacional do Petróleo (ANP/PRH-25).

Competing Interests

The authors have declared that no competing interests exist.

References

1. Cho JM, Ahn CI, Pang C, Bae JW. Fischer-Tropsch synthesis on Co/AlSBA-15: Effects of hydrophilicity of supports on cobalt dispersion and product distributions. Catal Sci Technol. 2015; 5: 3525-3535.
2. Espinoza RL, Steynberg AP, Jager B, Vosloo AC. Low temperature Fischer-Tropsch synthesis from a Sasol perspective. Appl Catal A Gen. 1999; 186: 13-26.
3. Vervloet D, Kapteijn F, Nijenhuis J, van Ommen JR. Fischer-Tropsch reaction-diffusion in a cobalt catalyst particle: Aspects of activity and selectivity for a variable chain growth probability. Catal Sci Technol. 2012; 2: 1221-1233.
4. Khodakov AY, Chu W, Fongarland P. Advances in the development of novel cobalt Fischer-Tropsch catalysts for synthesis of long-chain hydrocarbons and clean fuels. Chem Rev. 2007; 107: 1692-1744.
5. Calleja G, de Lucas A, van Grieken R. Co/HZSM-5 catalyst for syngas conversion: Influence of process variables. Fuel. 1995; 74: 445-451.
6. González O, Pérez H, Navarro P, Almeida LC, Pacheco JG, Montes M. Use of different mesostructured materials based on silica as cobalt supports for the Fischer-Tropsch synthesis. Catal Today. 2009; 148: 140-147.
7. de Sousa BV, Rodrigues MGF, Cano LA, Cagnoli MV, Bengoa JF, Marchetti SG, et al. Study of the effect of cobalt content in obtaining olefins and paraffins using the Fischer-Tropsch reaction. Catal Today. 2011; 172: 152-157.
8. Jahangiri H, Bennet J, Mahjoubi P, Wilson K, Gu S. A review of advanced catalyst development for Fischer-Tropsch synthesis of hydrocarbons from biomass derived syngas. Catal Sci Technol. 2014; 4: 2210-2229.
9. Kim NY, Jung JS, Lee JS, Yang EH, Hong GH, Lim SS, et al. Synthesis and characterization of Al-modified SBA-15 for Fischer-Tropsch synthesis (FTS) reaction. Res Chem Intermed. 2016; 42: 319-334.
10. Zhao D, Feng J, Huo Q, Melosh N, Fredrickson GH, Chmelka BF, et al. Triblock copolymer synthesis of mesoporous silica with periodic 50 to 300 angstrom pores. Science. 1998; 279: 548-552.
11. Zhang F, Yan Y, Yang H, Meng Y, Yu C, Tu B, et al. Understanding effect of wall structure on the hydrothermal stability of mesostructured silica SBA-15. J Phys Chem B. 2005; 109: 8723-8732.
12. Rodrigues JJ, Fernandes FAN, Rodrigues MGF. Study of Co/SBA-15 catalysts prepared by microwave and conventional heating methods and application in Fischer-Tropsch synthesis. Appl Catal A Gen. 2013; 468: 32-37.
13. Coronel-García MA, de La Torre AIR, Melo-Banda JA, Martínez-Salazar AL, Rodrigo RS, Díaz Zavala NPD, et al. Study of Co, Ru/SBA-15 type materials for Fischer-Tropsch synthesis in fixed bed tubular reactor: I. Effect of the high Ru content on the catalytic activity. Int J Hydrogen Energy. 2015; 40: 17264-17271.
14. Martínez A, Lopéz C. Fischer-Tropsch catalysts based on cobalt supported on ordered mesoporous silicas. Rev Mex Ing Quim. 2006; 5: 167-177.

15. van der Laan GP, Beenackers AACM. Hydrocarbon selectivity model for the gas-solid Fischer-Tropsch synthesis on precipitated iron catalysts. Ind Eng Chem Res. 1999; 38: 1277-1290.
16. Farias FEM, Silva FRC, Cartaxo SJM, Fernandes FAN, Sales FG. Effect of operating conditions on Fischer-Tropsch liquid products. Lat Am Appl Res. 2007; 37: 283-287.
17. Farias FEM, Sales FG, Fernandes FAN. Effect of operating conditions and potassium content on Fischer-Tropsch liquid products produced by potassium-promoted iron catalysts. J Nat Gas Chem. 2008; 17: 175-178.
18. Fernandes FAN, Sousa EMM. Fischer-tropsch synthesis product grade optimization in a fluidized bed reactor. AIChE J. 2006; 52: 2844-2850.
19. Mazzone LCA, Fernandes FAN. Modeling of Fischer-Tropsch synthesis in a tubular reactor. Lat Am Appl Res. 2006; 36: 141-148.
20. Visconti CG, Tronconi E, Lietti L, Zennaro R, Forzatti P. Development of a complete kinetic model for the Fischer-Tropsch synthesis over Co/Al_2O_3 catalysts. Chem Eng Sci. 2007; 62: 5338-5343.
21. Fernandes FAN. Modeling and product grade optimization of Fischer−Tropsch synthesis in a slurry reactor. Ind Eng Chem Res. 2006; 45: 1047-1057.
22. Fontenelle Jr AB, Fernandes FAN. Comprehensive polymerization model for fischer-tropsch synthesis. Chem Eng Technol. 2011; 34: 963-971.
23. Zhang WH, Lu J, Han B, Li M, Xiu J, Ying P, et al. Direct synthesis and characterization of titanium-substituted mesoporous molecular sieve SBA-15. Chem Mater. 2002; 14: 3413-3421.
24. Katiyar A, Yadav S, Smirniotis PG, Pinto NG. Synthesis of ordered large pore SBA-15 spherical particles for adsorption of biomolecules. J Chromatogr. 2006; 1122: 13-20.
25. Klimova T, Reyes J, Gutiérrez O, Lizama L. Novel bifunctional NiMo/Al-SBA-15 catalysts for deep hydrodesulfurization: Effect of support Si/Al ratio. Appl Catal A Gen. 2008; 335: 159-171.
26. Rodrigues JJ, Lima LA, Lima WS, Rodrigues MGF, Fernandes FAN. Fischer-Tropsch synthesis in slurry-phase reactores using Co/SBA-15 catalysts. Braz J Pet Gas. 2011; 5: 149-157.
27. Rodrigues JJ, Lima LA, Paula GM, Rodrigues MGF. Synthesis and characterization of molecular sieve SBA-15 and catalysts Co/SBA-15 and Ru/Co/SBA-15. Mater Sci Forum. 2014; 798: 100-105.
28. Rodrigues JJ, Pecchi G, Fernandes FAN, Rodrigues MGF. Ruthenium promotion of Co/SBA-15 catalysts for Fischer-Tropsch synthesis in slurry-phase reactors. J Nat Gas Chem. 2012; 21: 722-728.
29. Luan Z, Hartmann M, Zhao D, Zhou W, Kevan L. Alumination and ion exchange of mesoporous SBA-15 molecular sieves. Chem Mater. 1999; 11: 1621-1627.
30. Luan Z, Maes EM, van der Heide PAW, Zhao D, Czernuszewicz RS, Kevan L. Incorporation of titanium, into mesoporous silica molecular sieve SBA-15. Chem Mater. 1999; 11: 3680-3686.
31. Sing KSW. Reporting physisorption data for gas/solid systems with special reference to the determination of surface area and porosity (Recommendations 1984). Pure Appl Chem. 1985; 57: 603-619.
32. Leofanti G, Padovan M, Tozzola G, Venturelli B. Surface area and pore texture of catalysts. Catal Today. 1998; 41: 207-219.
33. Khalfaoui M, Knani S, Hachicha MA, Lamine AB. New theoretical expressions for the five adsorption type isotherms classified by BET based on statistical physics treatment. J Colloid Interface Sci. 2003; 263: 350-356.
34. Xiong H, Zhang Y, Liew K, Li J. Fischer-Tropsch synthesis: The role of pore size for Co/SBA-15 catalysts. J Mol Catal A. 2008; 295: 68-76.

35. Cruz MGA, Bastos-Neto M, Oliveira AC, Filho JM, Soares JM, Rodriguez-Castellon E, et al. On the structural, textural and morphological features of Fe-based catalysts supported on polystyrene mesoporous carbon for Fischer-Tropsch synthesis. Appl Catal A Gen. 2015; 495: 72-83.
36. Cruz MGA, de Oliveira APS, Fernandes FAN, de Sousa FF, Oliveira AC, Filho JM, et al. Fe-containing carbon obtained from ferrocene: Influence of the preparation procedure on the catalytic performance in FTS reaction. Chem Eng J. 2017; 317: 143-156.
37. Kuipers EW, Vinkenburg IH, Oosterbeek H. Chain length dependence of a-Olefin readsorption in Fischer-Tropsch synthesis. J Catal. 1995; 152: 137-146.
38. Martínez A, López C, Márquez F, Díaz I. Fischer-Tropsch synthesis of hydrocarbons over mesoporous Co/SBA-15 catalysts: The influence of metal loading, cobalt precursor, and promoters. J Catal. 2003; 220: 486-499.
39. Reuel RC, Bartholomew CH. The stoichiometries of H_2 and CO adsorptions on cobalt: Effects of support and preparation. J Catal. 1984; 85: 63-77.
40. Shiba NC, Liu X, Mao H, Qian X, Hildebrandt D, Yao Y. Effect of Ru-promotion on the catalytic performance of a cobalt-based Fischer-Tropsch catalyst activated in syngas or H_2. Fuel. 2022; 320: 123939.
41. Gahtori J, Singh G, Tucker CL, van Steen E, Biradar AV, Bordoloi A. Insights into promoter-enhanced aqueous phase CO hydrogenation over Co@TiO_2 mesoporous nanocomposites. Fuel. 2022; 310: 122402.
42. de Oliveira AHS, Aguiar EFS, Cavalcante CL. Production of liquid hydrocarbons via Fischer-Tropsch synthesis on a pilot-scale reactor using a cobalt-based mesoporous catalyst. Braz J Chem Eng. 2022. doi: 10.1007/s43153-021-00203-5.